Improved Optical Communications Performance Using Adaptive Optics with an Avalanche Photodiode Detector

M. W. Wright,[1] M. Srinivasan,[1] and K. Wilson[1]

We present predicted and experimentally measured gains in communications performance of a laboratory-based, free-space optical communications system through the use of adaptive optics (AO). A commercially available avalanche photodiode detector (APD) is used in the receiver for signal detection. Background noise and atmospheric turbulence field conditions were simulated in the laboratory using an integration sphere and a specially designed heater. At an uncoded bit-error rate (BER) of 0.3, a 5- to 6-dB gain in the received signal power is shown when AO correction is applied in the presence of high background and turbulence. The data stream was a 100-megabits per second (Mbps) pseudo-random bit sequence (PRBS), on–off-keying (OOK)-modulated, 1064-nm laser pulse train.

I. Introduction

Free-space optical communication through atmospheric turbulence suffers due to distortion of the signal field distribution in the detector focal plane and the spreading of the signal intensity. These aberrations result in spot sizes in the focal plane that are several times diffraction limited for the aperture and require larger photodetectors to capture the required number of signal photons for the desired link performance. For uniformly distributed sky background intensity, the larger detector collects proportionally more background photons and results in degraded link performance. In general, larger-area detectors limit the data rate realizable due to the lower bandwidths and can contribute to temporal distortion of the received signal. By using adaptive optics (AO) techniques, the atmosphere-induced wavefront aberrations can be corrected, and near-diffraction-limited focused spot sizes can be realized. This would enable the use of smaller, high-speed detectors with better spatial discrimination against the unwanted background noise.

Previous work has pointed to the benefits of AO in a turbulent laboratory optical communication system [1], but only low-order corrections were demonstrated with indirect bit-error rate (BER) measurements [2]. In [3], it was shown analytically that if an ideal photon-counting photodetector is used, AO can realize a gain of 1 to 6 dB over an uncompensated system in turbulent conditions for certain background levels and modulation formats. While there are several efforts that focus upon achieving photon-counting

[1] Communications Architectures and Research Section.

The research described in this publication was carried out by the Jet Propulsion Laboratory, California Institute of Technology, under a contract with the National Aeronautics and Space Administration.

detectors, these devices are not yet available to support data rates up to 100 Mbps, commensurate with deep space communications links. We therefore opted to use a commercially available silicon avalanche photodiode (APD) to evaluate the benefit that is realized by AO. In this article, we demonstrate AO performance in a laboratory AO communication test bed with an APD-detector-based receiver and compare the experimentally measured gains with the corresponding analytically predicted results for the APD channel.

Future demonstrations of free-space optical communications, such as the Mars Laser Communication Demonstration, are baselining photon-counting receivers, especially suitable for the photon-starved deep-space links. However, near-term field demonstrations over much shorter distances most likely will rely on commercial APD detectors. These tests will be used to establish the benefits of AO under real-world operating conditions.

The signal-to-noise ratio (SNR) enhancement afforded by AO is most significant in the presence of background noise either when the receiver is pointed close to the Sun or when the transmitter is in front of a bright source, as in the case of an optical communications probe orbiting Mars. The increased signal intensity in the presence of background irradiance facilitates the implementation of spatial filtering techniques that can enhance the SNR and, hence, the link performance.

II. APD Channel Model and Analytical Performance

Two modulation formats are considered here: pulse position modulation (PPM) and on–off keying (OOK). Optimal demodulation of PPM consists of integrating the APD output signal over each time slot and then choosing the slot with the largest value as that containing the transmitted signal pulse. While photoelectrons output from a photon-counting detector are Poisson distributed, the output of an APD is governed by the McIntyre–Conradi distribution [4], which we approximate with a Gaussian distribution [5]. The probability of bit error for M-ary PPM thus is given by

$$P_{\mathrm{PPM}}(E) = \frac{M}{2(M-1)} \int_{-\infty}^{\infty} \phi\left(x, \mu_s, \sigma_s^2\right) \left[1 - \Phi\left(\frac{x-\mu_b}{\sigma_b}\right)^{M-1}\right] dx \tag{1}$$

where $\phi\left(x, \mu, \sigma^2\right)$ is the Gaussian probability density function with mean μ and variance σ^2, and $\Phi(x)$ is the Gaussian distribution function. The means and variances of the integrated detector output charge for background and signal slots are given by

$$\mu_b = qGn_b + GI_bT_s + I_sT_s$$

$$\mu_s = qG(n_b + n_s) + GI_bT_s + I_sT_s$$

$$\sigma_b^2 = \left[2q^2G^2Fn_b + 2qG^2FI_bT_s + 2qI_sT + \frac{4\kappa TT_s}{R_L}\right] BT_s$$

and

$$\sigma_s^2 = \left[2q^2G^2F(n_b + n_s) + 2qG^2FI_bT_s + 2qI_sT + \frac{4\kappa TT_s}{R_L}\right] BT_s$$

Here, $F = kG + (2 - 1/G)(1 - k)$ is the APD excess noise factor, G is the average APD gain, k is the APD ionization ratio, q is the electron charge, κ is Boltzmann's constant, T is the equivalent noise temperature,

B is the single-sided noise bandwidth, R_L is the load resistance, I_b is the APD bulk dark current, and I_s is the APD surface leakage current. The mean numbers of absorbed background and signal photons are given by n_b and n_s, respectively, i.e.,

$$n_b = \eta \frac{q}{h\nu} P_b T_s$$

$$n_s = \eta \frac{q}{h\nu} \left(P_b + P_s\right) T_s$$

where $P_{b,s}$ is the background, or signal power, T_s is the slot time, and η is the detector quantum efficiency. The responsivity, $R_{res} = \eta q/(h\nu)$, also can be used.

For OOK modulation, optimal demodulation consists of setting a threshold on the integrated detector output over each slot to determine if a pulse was transmitted. With an optimized threshold and the same mean and variance parameters defined above, the probability of bit error for OOK is given by

$$P_{\mathrm{OOK}}(E) = 1 - \Phi\left(\frac{\mu_s - \mu_b}{\sigma_s + \sigma_b}\right) \tag{2}$$

The numerical analysis of AO performance presented here is similar to that detailed in [3]. The effect of turbulence upon the optical signal is modeled through a simplified atmospheric simulation, followed by numerical evaluation of the bit-error rates from Eqs. (1) and (2). Performance is characterized in terms of the uncoded bit-error rate as a function of AO complexity and the gains of AO systems over nominal reception with no AO compensation. In [3], a photon-counting focal-plane detector array whose elements could be selectively combined to optimize performance [6] was analyzed along with a single large square detector. Here, we analyze only a single large area circular detector.

Kolmogorov phase screens [7,8] were used to simulate the effect of atmospheric turbulence with Fried parameter $r_o = 7$ cm (at 1064 nm) on the focal-plane signal distribution. This corresponds to poor seeing, approximately 3-arcsec seeing at 532 nm, at the JPL Table Mountain Facility, where the Optical Communications Telescope Laboratory will be used to conduct field tests as well as support future mission opportunities. Other parameters included in the simulation were a 1-meter telescope aperture and 1-angstrom optical filter centered around a nominal signal wavelength of 1.064 μm. A sequence of AO systems with varying numbers of actuators was then simulated, ranging from no actuators (and hence no compensation) to as many as 200 actuators across the pupil diameter. These focal-plane intensities were used to scale the number of signal photons per signal pulse, n_t, detected over the entire focal plane. For the purposes of this study, it is assumed that n_t is constant from pulse to pulse.

In [3], background photon levels from three different values of spectral radiance were assumed, corresponding to vastly different background conditions and environments [9,10]. For the purpose of a laboratory validation of AO communications performance with a silicon APD, signal and background levels were changed substantially to arrive at an operating region of interest. Based on the optical design of the test bed and using an integrating sphere to simulate the background noise, background and signal powers were varied to obtain uncoded bit-error rates from 0.3 to approximately 10^{-6}. The conversion of the signal and background power levels to the mean number of signal and background photons per slot depends upon the photodetector size, the data rate, and the PPM order or OOK slot width used. Because the photodetector size is optimized in the simulations for the number of actuators used in the AO system, the mean number of background photons per slot varies; hence, we provide the background photon levels per diffraction-limited field of view, or pixel, which we denote by Δn_b. At a data rate of 100 megabits per second (Mbps) and an incident background power of 18 nW, the values of Δn_b were calculated to be 16.6

for OOK, 4.16 for 16-PPM, and 1.56 for 64-PPM. The actual average number of background photons per slot then is calculated from these numbers by summing over the number of diffraction-limited pixels in the detector, whose size is optimized for the particular operating point being considered and is therefore variable.

The results of this analytical performance evaluation are presented in Figs. 1 through 3. Figure 1(a) shows the uncoded BER, as a function of the signal power incident upon the detector, for OOK at 100 Mbps. The curves are shown for selected values of n, the numbers of actuators across the pupil to correct wavefront error: $n = 0$, $n = 11$, $n = 31$, and finally the case of no wavefront error. We note that the $n = 11$ AO system improves the performance of the uncompensated $n0$ system by about 3 dB at a 0.3 BER. The $n = 31$ AO system results in an improvement of 6 dB, which is about 0.5 dB short of the limiting performance (at 0.3 BER) corresponding to no wavefront error. Figure 1(b) shows the same bit-error rates as Fig. 1(a), but now as a function of the number of actuators across the pupil, for the three values of signal power of −57 dBm, −52 dBm, and −47 dBm. The practical limit of what may be currently implemented in a 1-meter telescope corresponds to $n = 31$ actuators.

Figures 2 and 3 show analogous results for 16-PPM and 64-PPM, assuming the same fixed data rate of 100 Mbps. As the PPM order increases and the data rate is fixed, the slot size decreases. The results for all three modulation orders are distilled in Fig. 4, in which the gains of specific AO systems at the uncoded BER of 0.3 are plotted for all three background cases. We observe that the AO gains are consistent across modulation formats. This is unlike the photon-counting results presented in [3], in which higher-order modulation and small slot widths resulted in significantly lower gains.

III. Experiment

The AO optical communication test bed is described in detail in [11,12] and shown for reference in Fig. 5. The transmit channel consists of various fiber-coupled laser sources at 1064 nm that can be modulated to greater than 100 Mbps and a beacon simulator at 635 nm. The receive channel consists of a free-space-coupled APD module along with a scoring camera to monitor the spot size of the corrected and uncorrected beams. Also included is an integrating sphere to generate the appropriate signal to

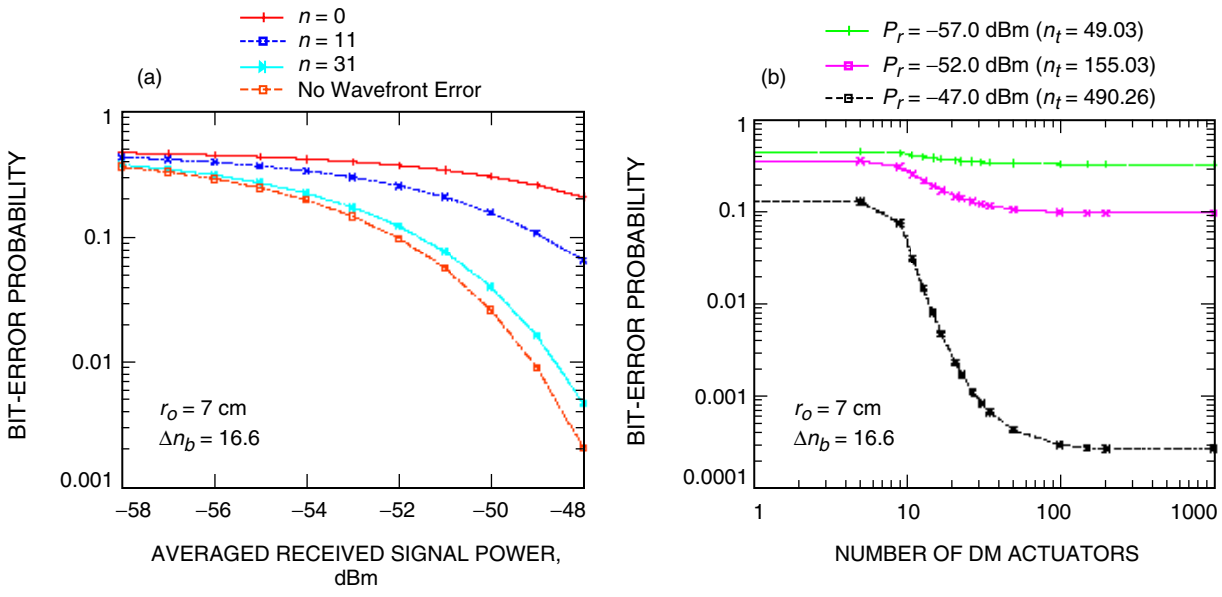

Fig. 1. Bit-error rates for OOK at 100 Mbps: (a) BER versus the total received signal power in the focal plane for various AO systems and (b) BER versus the number of DM actuators across the pupil, for specific signal photon levels.

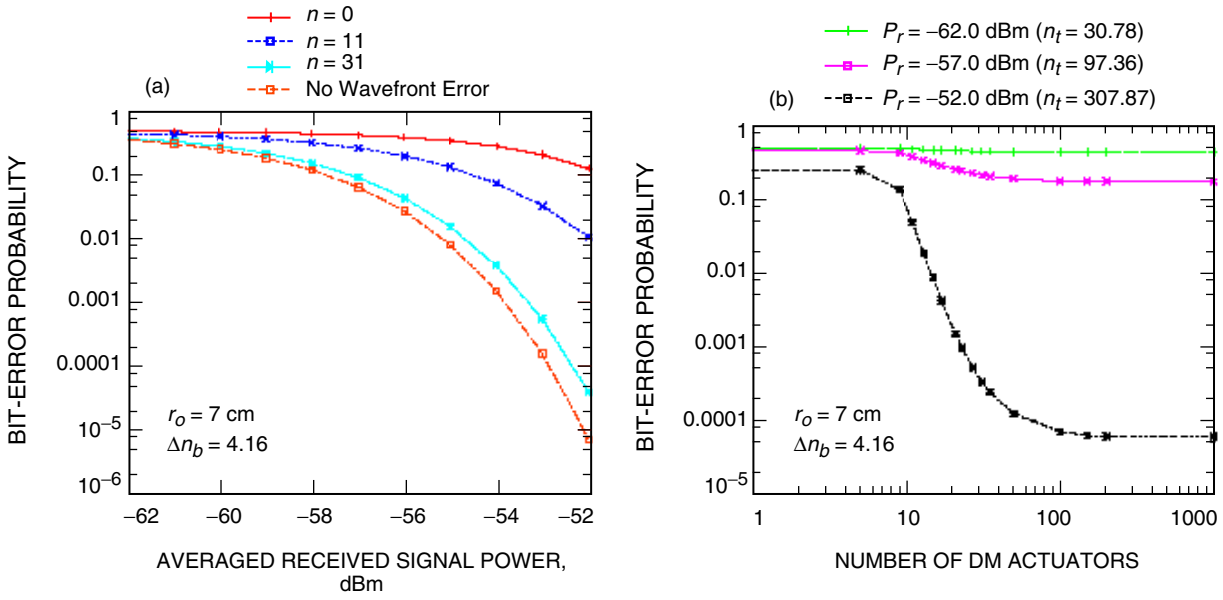

Fig. 2. Bit-error rates for 16-PPM at 100 Mbps: (a) BER versus the total received signal power in the focal plane for various AO systems and (b) BER versus the number of DM actuators across the pupil, for specific signal photon levels.

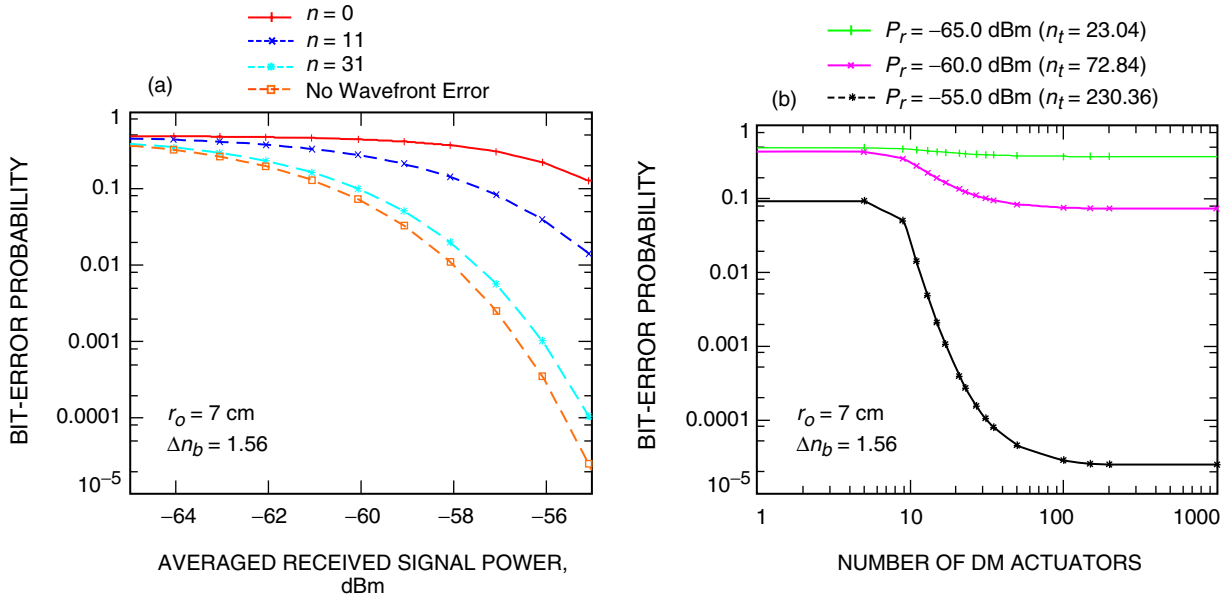

Fig. 3. Bit-error rates for 64-PPM at 100 Mbps: (a) BER versus the total received signal power in the focal plane for various AO systems and (b) BER versus the number of DM actuators across the pupil, for specific signal photon levels.

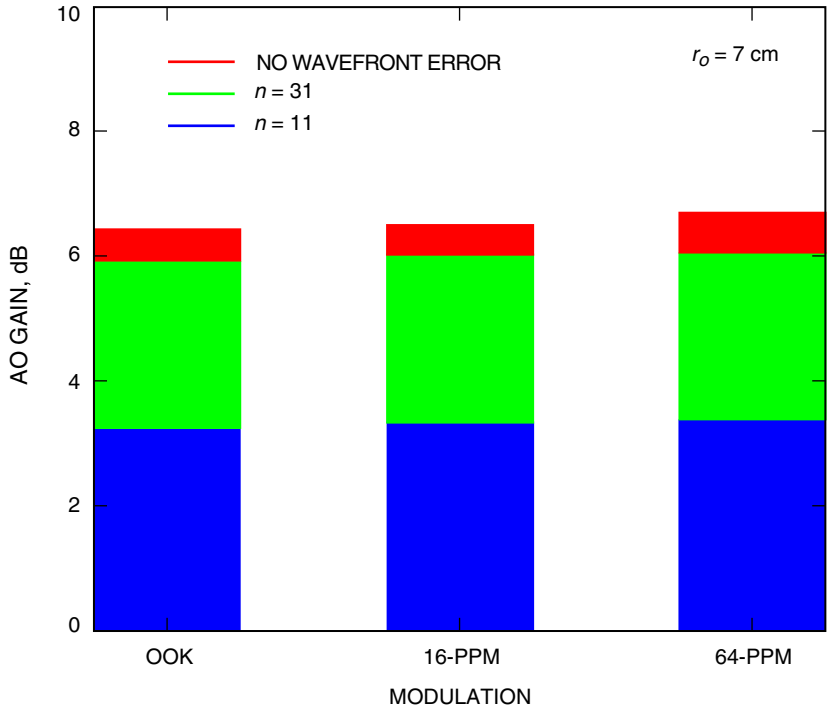

Fig. 4. Performance gains of AO systems at a 0.3 BER with a silicon APD detector at 100-Mbps modulation.

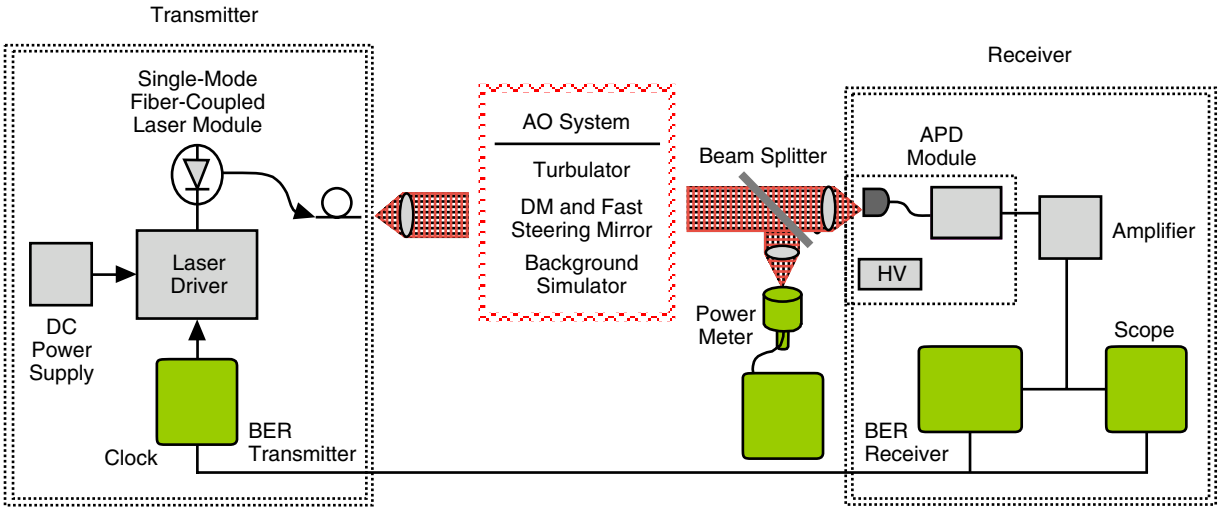

Fig. 5. Laboratory test setup.

simulate the sky background. A zoom capability is used to vary the receive signal spot size and, hence, power. Strictly speaking, the background simulator should be placed before the zoom so the background strength could be varied as the spot size is scaled. However, in order to obtain sufficient background signal strength with the APD detector, it was placed after the zoom. The background power level then could be varied independently by adjusting the current to the integrating sphere lamp. The transmit power could be varied either by adjusting the laser bias and modulation current or by placing variable neutral density (ND) filters in the optical path. The beam splitter in the received path is used to calibrate the received power independently with a separate power meter. The received power on the actual data detector was inferred by assuming a Gaussian spot with the measured full width at half maximum (FWHM) and correcting for the detector diameter. At high data rates, the bias point of the laser generally is set near the threshold current for optimal performance. We made minor adjustments to the bias point and modulation current depth to optimize the quality of the modulated signal.

In the experiment, two lasers were tested. The first was a Lumics fiber-coupled diode laser with an external fiber Bragg grating (FBG) that produced single-frequency operation, and the second was a conventional fiber-coupled diode with a back-matched driving source from Microlaser. Care was taken to ensure DC coupling of the laser drive current to avoid drift in the on or off state with long periods of consecutive identical bits. The emitter-coupled logic (ECL)-type modulated signal was provided by a pseudo-random bit sequence (PRBS) pattern of word length PN 7. The detector was a 500-μm infrared (IR)-enhanced Hamamatsu APD detector, integrated with a transimpedance amplifier (TIA) and high-voltage (HV) supply in a standard module. The APD high voltage gain was adjusted to optimize the BER in the given setup. The BERs were measured with a MicroLogic BER test set, usually averaged for several seconds, as a function of received power. The parameters of the APD are given in Table 1.

Table 1. APD parameters.

Parameter	Value
Ionization coefficient, k	0.02
Gain, M	80
Response, R_{res}	0.2 A/W
Load resistance, R_L	10,000 Ω
Noise temperature	4174 K
Bandwidth, B	100 MHz
Bulk dark current	0.3 nA
Surface leakage current	0.0 A

IV. Laboratory Test Results

Figure 6 shows OOK bit-error rates measured with the detector placed directly after the transmit channel. This was used to compare with the theoretical BER values from Eq. (2), using the parameter values from Table 1. The 1- to 2-dB difference shown in Fig. 6 can be attributed to variations in the noise temperature or the APD gain setting.

With the transmitter and receivers placed in the AO test bed, turbulence and background light were introduced in a controlled fashion. Calibration of the optical path—in particular, the received spot size with zoom setting—was shown in [11]. For a received signal power level of approximately −40 dBm and a zoom setting of "2," the BER was measured as a function of the background light. Figure 7 shows that, with a maximum luminance of nearly 6000 fL or 40 nW incident on the detector, the BER degrades by an

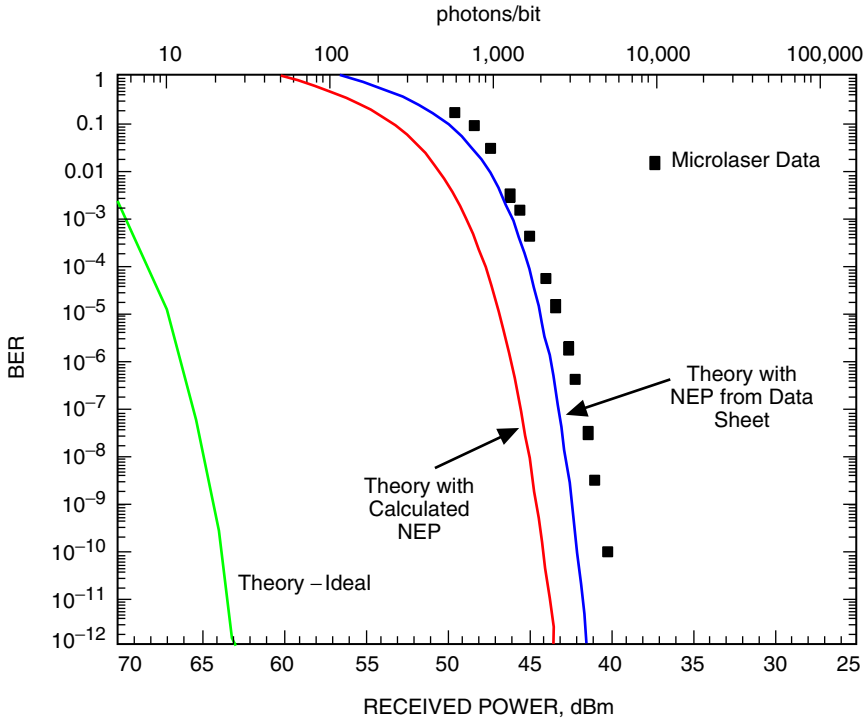

Fig. 6. Theoretical and experimental OOK bit-error probabilities for a silicon APD. The ideal curve corresponds to a non-APD detector with Poisson-distributed receive statistics. The calculated noise equivalent power uses a noise temperature of 300 K, and the NEP from the data sheet gives a noise temperature of approximately 1160 K.

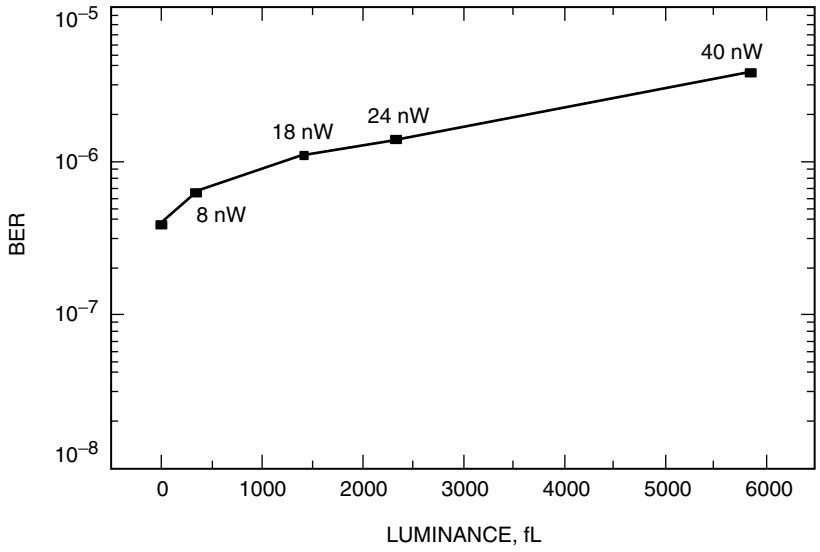

Fig. 7. BER as a function of uniform background noise level. The values represent the approximate power incident on the actual detector through the 25-nm filter centered at 1064 nm. The zoom setting was at "2" or an FWHM spot size of ~100 μm.

order of magnitude. Assuming a detector field of view of 200 μrad on the 1-m telescope, with 50 percent transmittance, this condition corresponded to a sky irradiance of approximately 9.10^4 μW/sr/nm or a Sun–Earth–probe (SEP) angle of 2 to 3 degrees. Keeping the background level at the maximum and with a similar received signal power level of −40 dBm, the turbulence was added by turning on the heater plate in the turbulator. As the turbulator warmed up, hot air formed convective patterns that caused scintillation effects in the propagated beam. The characterization of the system in terms of the atmospheric parameter r_o was shown in [11]. The effect on the BER is shown in Fig. 8 as a function of turn-on time or effective r_o for a zoom setting of "4." The AO correction was also enabled by activating the deformable mirror (DM) and tip–tilt mirror, and is shown as the lower curve. After approximately 40 minutes, the system is saturated, so where the performance at various received power levels was compared, the BERs were always measured after this time between setting changes. The AO correction improved the BER by over two orders of magnitude. However, there was still some residual wavefront error uncorrected by the DM and tip–tilt mirrors. This residual difference is due to non-common path errors between the wavefront sensor camera and the scoring camera optical channels. We believe that this could be reduced by further calibration. A higher closed-loop bandwidth for the DM would also allow the system to track the turbulent effects with a faster response time and improve the AO correction. During heater turn-on, the received spot was also monitored through a 25-nm narrowband filter. The data are plotted in Fig. 9 with and without the DM loop closed at a zoom setting of "4." The increased spot was averaged over several seconds with frames taken at approximately 30 Hz. Examples of the actual received signals with and without AO correction are shown in the insets of the graph on the same scale. Given the 500-μm detector diameter and simulating the turbulent beams as Gaussian with the indicated FWHM diameter, the reduction in received power correlates well with the reduction in BER of Fig. 8.

Once the turbulence had reached saturation, the zoom was fixed at a setting of "2," and the transmit power was varied to give the BER as a function of received power, shown in Fig. 10. The received power was calibrated by placing a power meter in the scoring camera location in the receive channel when no background signal was present. At each power level, the DM loop was opened and closed for several seconds until the BER stabilized. For comparison, the BER with no turbulence is also shown as

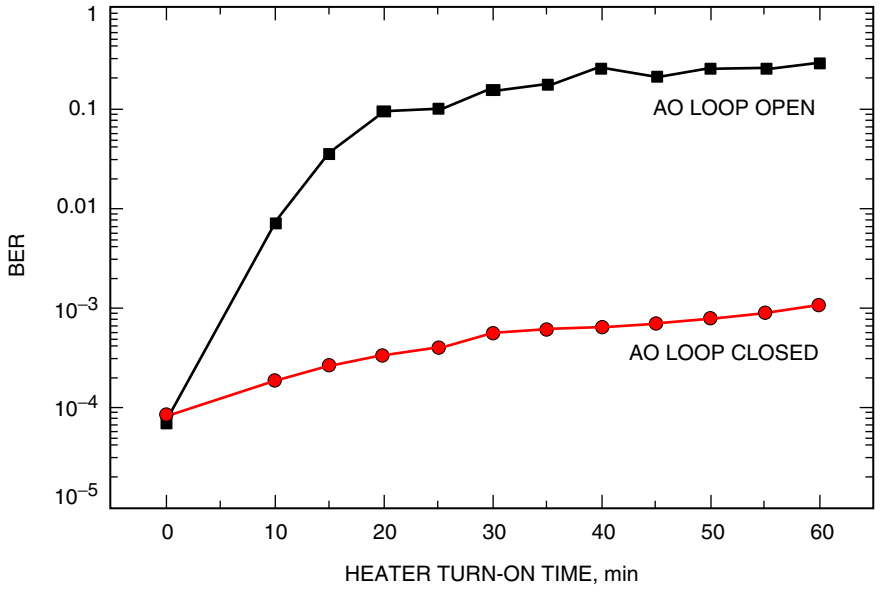

Fig. 8. BER as a function of heater turn-on time with zoom setting "4" (no turbulence spot size ~220 μm) and 40 nW (20 μW/cm^2) of background noise level. The saturated r_o ~ 9 mm.

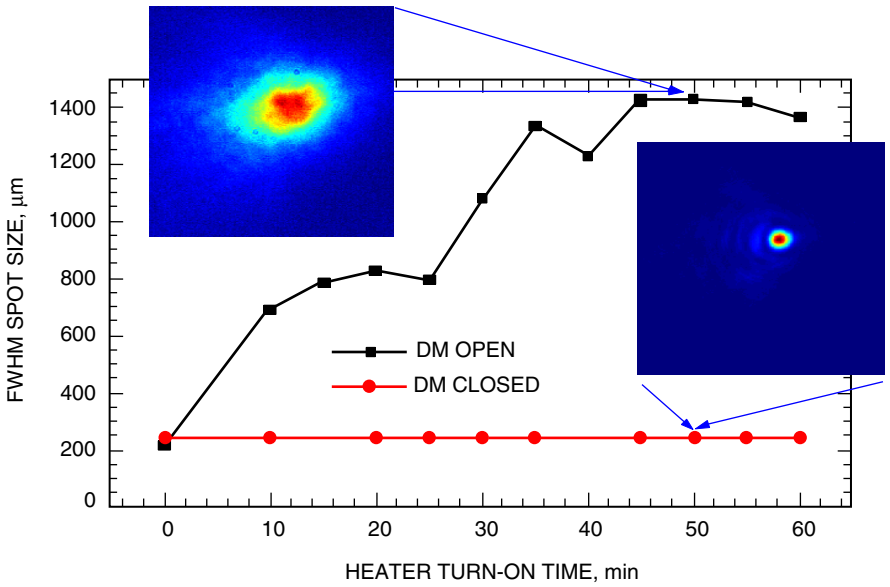

Fig. 9. Spot size as a function of turbulence as determined by heater turn-on time with zoom setting "4." The saturated r_o ~ 9 mm and the spot sizes are on the same scale.

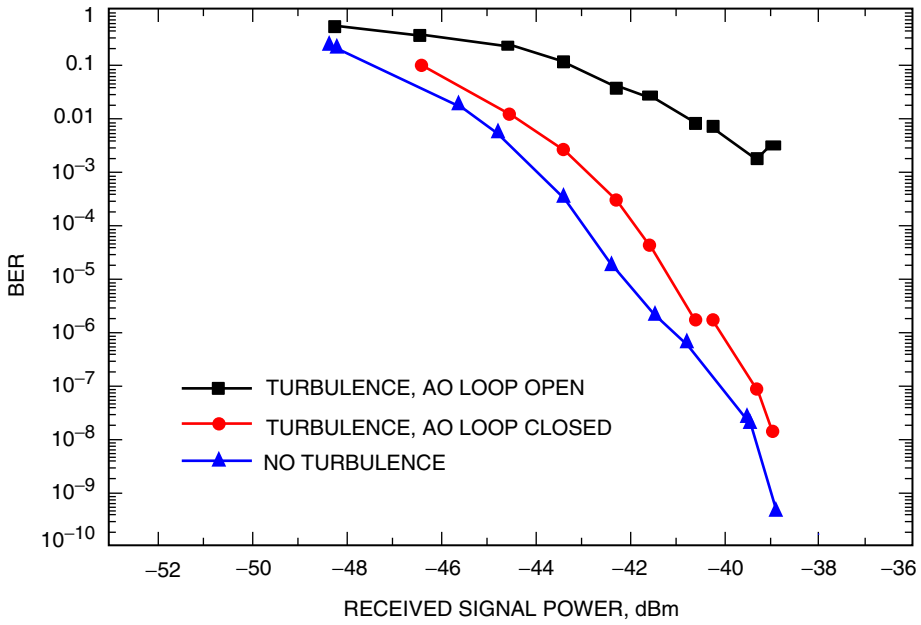

Fig. 10. BER as a function of received signal for a zoom setting of "2" with no background signal. The turbulence corresponded to an r_o ~ 9 mm.

reference. Similar gains in received signal sensitivity also were demonstrated with a zoom setting of "4" and are shown in Fig. 11. Here, the maximum background signal was also added. Again it can be seen that the AO correction is not able to compensate fully for the turbulence with BERs slightly above the no-turbulence condition.

V. Discussion

The experimental results are now compared with analytically predicted results. Figure 12 shows the data with a zoom setting of "4" and high background, along with analytical data obtained as in Section II. However, the incident background level was increased to 40 nW to match that used in the experiment. The turbulence corresponded to an r_o of approximately 13 cm on the sky with approximately 91 actuators. Even though these results are preliminary, excellent agreement in the gain from the AO correction of 5 to 6 dB is demonstrated. Differences still remain between the experiment and the simulation. In particular, the experimental background levels were constant, whereas the analytical values varied slightly as the AO correction was incorporated. Hence, the close agreement between the two sets of results must be further validated to ensure the repeatability of these results.

It is known that tip/tilt is the major contribution to the wavefront distortion. Yet, correction of the higher-order wavefront errors provides for an instantaneous Airy diffraction pattern. In our experiment, the short optical path through the heated air column does not contribute significant tip/tilt distortion to the optical wavefront, and tip/tilt mirror corrections were minimal. However, the turbulator distorted the optical path enough that we measured an r_o of 9 mm in the 70-mm (D) optical beam at the highest turbulator settings. The value of D/r_o in the experiment corresponds to an r_o of 13 cm at 1064 nm on the sky. With AO enabled, the signal previously dispersed into several spatial modes by turbulence was now concentrated into a near-diffraction-limited spot. This increased the signal intensity at the detector. To simulate turbulent conditions in the laboratory comparable to the worst that could be seen in the field, the on-sky r_o needs to be decreased to around 3 cm or approximately 2 mm in the laboratory.

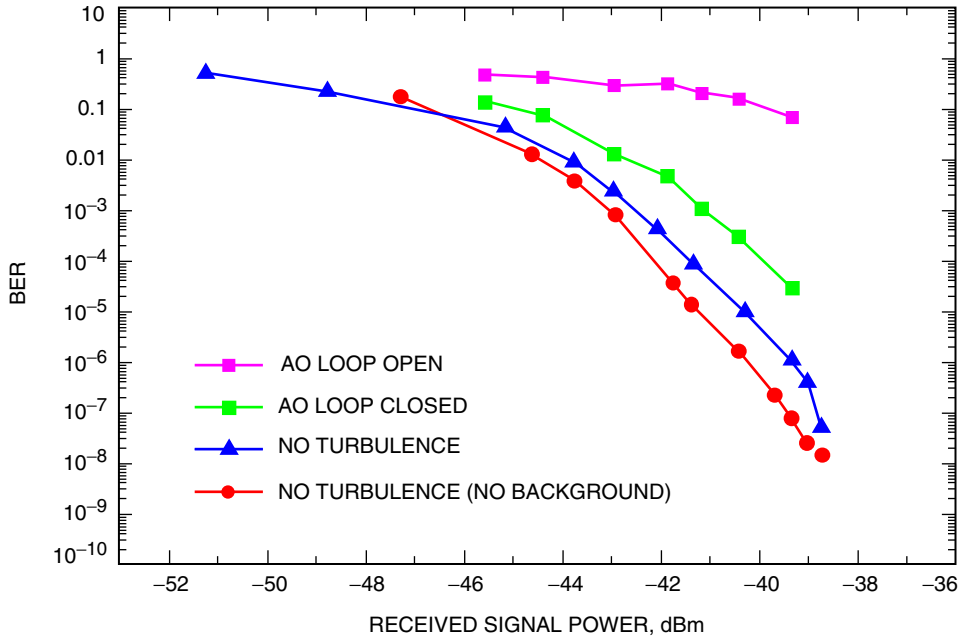

Fig. 11. BER as a function of received signal for a zoom setting of "4" with background set at a maximum of 40 nW incident on the detector except the lower curve, where the background was turned off. The turbulence corresponded to r_o = 9 mm.

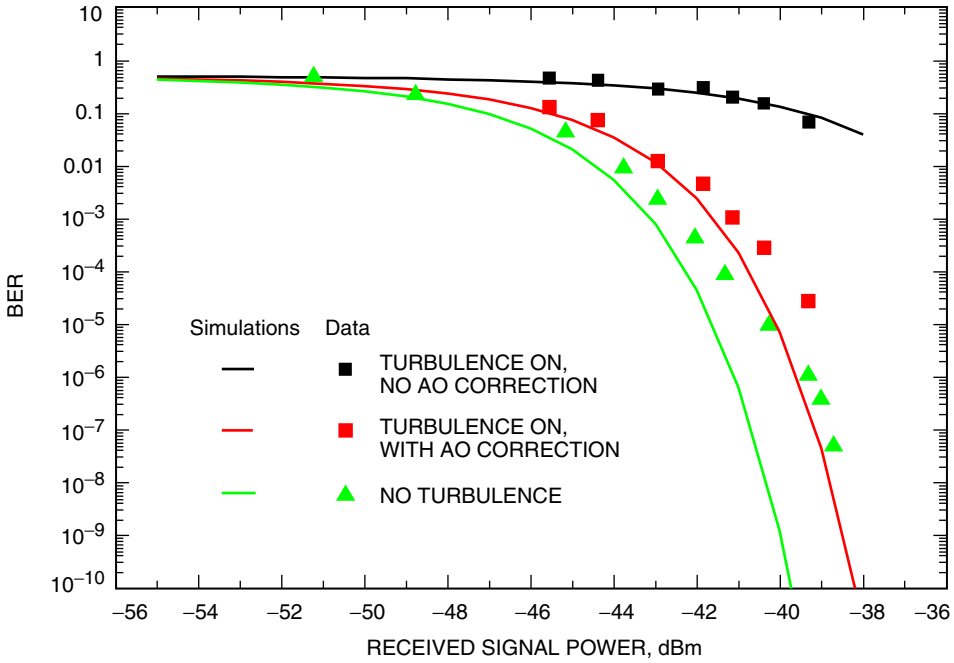

Fig. 12. Comparison of experimental data and simulations with turbulence and the DM loop open and closed. The turbulence corresponded to r_o = 9 mm and a background level of 40 nW on the detector.

VI. Conclusions

A free-space optical communications test bed has been built and tested; it incorporates an atmospheric turbulence simulator consisting of a perforated heated plate and an AO correction system. The wavefront sensor detected beam distortions and corrected the beam profile by commanding a 91-actuator deformable mirror and fast tip–tilt mirror. The gain in communications performance was verified with a 100-Mbps OOK data stream incident onto a silicon APD detector. The experimental arrangement served as a laboratory test bed for deep-space optical communications and demonstrated over 5 dB of signal gain, in agreement with numerical simulations. Further work will investigate the performance enhancement of a PPM modulation scheme with the eventual goal of integrating a photon-counting detector, as is baselined for a deep-space optical link.

References

[1] R. K. Tyson, "Bit Error Rate for Free Space Adaptive Optics Laser Communications," *J. Opt. Soc. Am. A*, vol. 19, no. 4, pp. 753–758, April 2002.

[2] R. K. Tyson and D. E. Canning, "Indirect Measurement of a Laser Communications Bit Error Rate Reduction with Low Order Adaptive Optics," *App. Opt.*, vol. 42, no. 21, pp. 4239–4243, July 2003.

[3] M. Srinivasan, V. Vilnrotter, M. Troy, and K. Wilson, "Adaptive Optics Communications Performance Analysis," *The Interplanetary Network Progress Report*, vol. 42-158, Jet Propulsion Laboratory, Pasadena, California, pp. 1–14, August 15, 2004. http://ipnpr.jpl.nasa.gov/tmo/progress_report/42-158/158B.pdf

[4] R. J. McIntyre, "The Distribution of Gains in Uniformly Multiplying Avalanche Photodiodes: Theory," *IEEE Transactions on Electron Devices*, vol. ED-19, no. 6, pp. 703–713, June 1972.

[5] F. M. Davidson and X. Sun, "Gaussian Approximation Versus Nearly Exact Performance Analysis of Optical Communications Systems with PPM Signaling and APD Receivers," *IEEE Transactions on Communications*, vol. COM-36, no. 11, pp. 1185–1192, November 1988.

[6] V. Vilnrotter and M. Srinivasan, "Adaptive Detector Arrays for Optical Communications Receivers," *IEEE Transactions on Communications*, vol. 50, no. 7, pp. 1091–1097, July 2002.

[7] L. C. Andrews and R. L. Phillips, *Laser Beam Propagation through Random Media*, Bellingham, Washington: SPIE Optical Engineering Press, 1998.

[8] P. Negrete-Regagnon, "Practical Aspects of Image Recovery by Means of the Bispectrum," *JOSA*, vol. 13, no. 7, pp. 1557–1576, July 1996.

[9] R. A. Oetjen, E. E. Bell, J. Young, and L. Eisner, "Spectral Radiance of Sky and Terrain at Wavelengths Between 1 and 20 Microns. I. Instrumentation," *JOSA*, vol. 50, issue 12, pp. 1308–1313, December 1960.

[10] J. V. Sandusky, D. J. Hoppe, and M. J. Britcliffe, "Deep-Space Optical Reception Antenna (DSORA): Aperture Versus Quality," *The Telecommunications and Mission Operations Progress Report 42-143, July–September 2000*, Jet Propulsion Laboratory, Pasadena, California, pp. 1–11, November 15, 2000. http://tmo.jpl.nasa.gov/tmo/progress_report/42-143/143C.pdf

[11] M. Troy, J. Roberts, S. Guiwits, S. Azevedo, S. Bikkannavar, G. Brack, V. Garkanian, D. Palmer, B. Platt, T. Truong, K. Wallace, and K. Wilson, "Performance of the Optical Communication Adaptive Optics Testbed," *The Interplanetary Network Progress Report*, vol. 42-161, Jet Propulsion Laboratory, Pasadena, California, pp. 1–12, May 15, 2005. http://ipnpr.jpl.nasa.gov/tmo/progress_report/42-161/161A.pdf

[12] K. Wilson, M. Troy, M. Srinivasan, B. Platt, V. Vilnrotter, M. Wright, V. Garkanian, and H. Hemmati, "Daytime Adaptive Optics for Deep Space Optical Communications," *Proceedings of 10th ISCOPS Conference*, Tokyo, Japan, December 11, 2003.